# Synthesis of $Cu_yMn_zAl_{1-z}O_x$ mixed oxide as low-temperature $NH_3$-SCR catalyst with enhanced catalytic performance

Qinghua Yan[1], Sining Chen[1], Lei Qiu[1], Yanshan Gao[1], Dermot O'Hare[2], Qiang Wang[1,*]

[1]College of Environmental Science and Engineering, Beijing Forestry University, 35 Qinghua East Road, Haidian District, Beijing 100083, P. R. China

[2]Chemistry Research Laboratory, Department of Chemistry, University of Oxford, 12 Mansfield Road, Oxford, OX1 3TA, UK

*Corresponding author:

College of Environmental Science and Engineering, Beijing Forestry University, 35 Qinghua East Road, Haidian District, Beijing 100083, P. R. China

E-mail: qiang.wang.ox@gmail.com; qiangwang@bjfu.edu.cn

Tel: +86 13699130626

**Abstract**

A new type of low-temperature selective catalytic reduction (SCR) catalyst $Cu_yMn_zAl_{1-z}O_x$ derived from layered double hydroxides was designed. By tuning the ratio of Cu/Mn/Al, the optimal $NH_3$-SCR performance was achieved with the chemical composition of $Cu_2Mn_{0.5}Al_{0.5}O_x$. At 150 °C, a high $NO_x$ conversion of 91.2% was achieved with $Cu_2Mn_{0.5}Al_{0.5}O_x$, which is much higher than that of all other control catalysts $Cu_2AlO_x$ (71.1%), Cu-Mn/γ-$Al_2O_3$ (65.23%), and Mn/γ-$Al_2O_3$ (59.32%). Catalysts were characterized in detail using various physico-chemical techniques including XRD, BET, FTIR, TEM, $H_2$-TPR, $NH_3$-TPD, and XPS analyses, and the results revealed that the superior catalytic performance of $Cu_2Mn_{0.5}Al_{0.5}O_x$ catalyst can be attributed to its high specific surface area, high reducibility of $MnO_2$ and CuO species, abundance of surface acid sites, and well dispersion of $MnO_2$ and CuO species. $Cu_2Mn_{0.5}Al_{0.5}O_x$ also showed much higher resistance to 100 ppm $SO_2$ and 5% $H_2O$ than the control catalysts. The poisoning mechanism and the regenerability of $Cu_2Mn_{0.5}Al_{0.5}O_x$ catalyst was also investigated. In all, compared with the control catalysts of $Cu_2AlO_x$, Cu-Mn/γ-$Al_2O_3$, and Mn/γ-$Al_2O_3$, the newly designed $Cu_2Mn_{0.5}Al_{0.5}O_x$ catalyst is not only more active at low temperatures (100–250 °C), but also relatively more robust in the presence $SO_2$ and $H_2O$.

**Keywords:** selective catalytic reduction; Mn-based catalyst; layered double hydroxides; sulfur dioxide; regenerability

## 1. Introduction

The emissions of nitrogen oxides ($NO_x$) from power plant and municipal solid waste (MSW) incineration plant are known to cause damages to human health and environmental safety. The removal of nitrogen oxides from the flue gas has become an important issue. As the most effective method for the abatement of $NO_x$ emission from stationary resources, selective catalytic reduction (SCR) process has been put into widely commercial utilization during the past several decades.[1, 2]

The backbone of SCR technology is the development of SCR catalysts such as noble metals based,[3] supported metal oxides based,[4] zeolites based,[5] and many others.[6-8] Among them, vanadia-based catalyst is known to be the most effective and widely used commercial SCR catalyst due to its high activity and durability to $SO_2$. Because this catalyst exhibits good performance only in a narrow temperature window of 300–400 $^oC$, the SCR unite should be applied before units for electrostatic precipitator and desulphurization in order to avoid reheating of the flue gas.[9] However, the flue gas from incinerators has high concentrations of particles and other contaminants which cause the deactivation of catalysts. Therefore, for this reason, there is a strong interest in the development of SCR catalysts at lower temperatures (< 300 $^oC$). Low-temperature SCR catalysts would be placed downstream the desulfurizer and electrostatic precipitator, and the temperature at this point is 150−160 $^oC$. Success in developing such catalysts would significantly improve the economics of SCR. Moreover, there is still residual $SO_2$ remaining after the desulfurizer. Thus, $SO_2$ resistance needs to be considered as well.

To date, a large number of catalysts consisted of various transition metal (V, Cr, Mn, Fe, Co, Ni and Cu) oxides on different commercial supports such as titania and alumina have been studied for low temperature SCR reactions. Among these catalysts,

Mn-based catalysts such as $MnO_x/Al_2O_3$,[10] $MnO_x$/NaY,[11] $MnO_x$/USY,[12] and $MnO_x/TiO_2$[13, 14] have attracted interest because of its high SCR activity at low temperature. The manganese oxides contain various types of labile oxygen, which is necessary to complete oxidation–reduction cycle.[15, 16] However, Mn-based SCR catalyst still suffers the deactivation by $SO_2$. In order to enhance the SCR activity and $SO_2$ resistance of Mn-based catalyst, several transition metals (such as Ni, Ce, Cu, Fe, Co, etc.) have been used to modify the Mn-based catalysts.[17-22] Recently, Cu-based catalyst have received much attention due to its capability of simultaneous removal of $SO_2$ and $NO_x$ from flue gases. [23, 24] Therefore, In order to enhance the SCR activity and $SO_2$ resistance of Mn-based catalysts, copper transition metal be considered introducing to modify the Mn-based catalysts. In addition, there were some investigations on the synthesis of highly dispersed mixed metal oxides based catalysts via the careful calcination of a highly dispersed layered double hydroxides (LDHs) precursors.[25] Using this approach the dispersion of active metal species can be controlled at the atomic level.[26-29]

In the present work, we report a new low-temperature SCR catalyst $Cu_yMn_zAl_{1-z}O_x$ from CuMnAl-$CO_3$ LDH with enhanced SCR activity and $SO_2$ resistance. Synthesized catalyst were characterized using XRD, BET, SEM, TEM, FTIR, XPS, $NH_3$-TPD, and $H_2$-TPR in order to illustrate the influence of Cu modification and the advantages of using LDH precursor. The optimized catalyst with a composition of $Cu_2Mn_{0.5}Al_{0.5}O_x$ exhibited a $NO_x$ conversion as high as 91.2% at 150 $^oC$. It also showed higher $SO_2$ resistance than the control catalysts $Cu_2AlO_x$ LDO, Cu-Mn/$\gamma$-$Al_2O_3$, and Mn/$\gamma$-$Al_2O_3$. The influence of $H_2O$ on the catalytic activity of $Cu_2Mn_{0.5}Al_{0.5}O_x$ catalyst was also evaluated. We hope that this work could guide us to design highly efficient Mn-based SCR catalysts with excellent low-temperature activity and $SO_2$ resistance.

## 2. Experimental

### 2.1 Preparation of $Cu_yMn_zAl_{1-z}O_x$ ($y$ = 1–4) and $Cu_2AlO_x$ mixed oxide catalysts

For the synthesis $Cu_yMn_zAl_{1-z}$-$CO_3$ LDHs, a standard co-precipitation method was used. An aqueous solution containing nitrates of the metallic salts $Cu(NO_3)_2 \cdot 6H_2O$, $Al(NO_3)_3 \cdot 9H_2O$, and 50% $Mn(NO_3)_2$ with different $M^{2+}/M^{3+}$ ratios (1, 2, 3, and 4) and different $Mn^{3+}/Al^{3+}$ ratios (1:1, 1:3, and 3:1) was added dropwise into a vigorously stirred $Na_2CO_3$ solution. During the synthesis, the temperature of mixture solution was maintained at 60 $^oC$ and the pH of the mixture solution was kept constant at 10 by addition of NaOH solution (4 M). The resulting slurry was stirred continuously for about 12 h at 60 $^oC$. After aging, the precipitate was filtered and washed several times with deionized water until pH=7, then stirred in acetone for 2 h and washed with acetone. Finally, $Cu_yMn_zAl_{1-z}$-$CO_3$ LDHs were obtained by drying at 60 $^oC$ for 24 h in an oven. After being calcined at 400 $^oC$ for 5 h in air, various $Cu_yMn_zAl_{1-z}O_x$ mixed oxides were obtained, which were denoted as $Cu_1Mn_{0.5}Al_{0.5}O_x$, $Cu_2Mn_{0.5}Al_{0.5}O_x$, $Cu_3Mn_{0.5}Al_{0.5}O_x$, $Cu_4Mn_{0.5}Al_{0.5}O_x$, $Cu_2Mn_{0.25}Al_{0.75}O_x$, and $Cu_2Mn_{0.75}Al_{0.25}O_x$. Cu-Al-$CO_3$ LDH and the corresponding LDO $Cu_2AlO_x$ can be obtained similarly.

### 2.2 Preparation of Mn/γ-$Al_2O_3$ and Cu-Mn/γ-$Al_2O_3$ catalysts

For comparison, the Mn/γ-$Al_2O_3$ and Cu-Mn/γ-$Al_2O_3$ catalysts were prepared by a conventional incipient wetness impregnation method. For Mn/γ-$Al_2O_3$, 2 wt% Mn was loaded on the γ-$Al_2O_3$ carrier. 2.5 g γ-$Al_2O_3$ solid was impregnated with 10 mL aqueous solution containing 0.2 mL $Mn(NO_3)_2$. For Cu-Mn/γ-$Al_2O_3$, the molar ratio of Cu/Mn was fixed at 4:1. 2.5 g γ-$Al_2O_3$ solid was impregnated with 10 mL aqueous solution containing 0.2 mL $Mn(NO_3)_2$ and 0.88 g $Cu(NO_3)_2 \cdot 6H_2O$. Subsequently, the impregnated samples were first dried at 60 $^oC$ for 24 h in an oven, followed by

calcination at 400 $^{o}$C in air for 5 h. The loadings of Cu and Mn metals are based on γ-$Al_2O_3$ support.

### 2.3 Characterization of catalysts

X-ray powder diffraction (XRD) patterns of the as-synthesized and calcined samples were measured using a Shimadzu XRD-7000 instrument in reflection mode using Cu Kα radiation. The X-ray tube was operated at 40 kV and 40 mA. The accelerating voltage was set at 40 kV with 30 mA current (λ = 1.542 Å). Diffraction patterns were recorded within the range of 2θ = 5–75$^{o}$ with a scanning rate of 5$^{o}$/min and a step size of 0.02$^{o}$. The morphology of samples was characterized using field emission scanning electron microscope (FE-SEM, SU-8010, Hitachi). Fourier transform infrared spectrometer (FT-IR) experiments were performed on a FTS 3000 MX FT-IR (Bruker Vertex 70) spectrophotometer in the range of 4000 to 400 $cm^{-1}$ using the diamond ATR technique. One hundred scans were taken with a resolution of 4 $cm^{-1}$ and all spectra were background corrected. Specific surface areas (SSA) of samples were measured with a physisorption analyser (SSA–7000, Builder). Before each measurement, about 0.1 g catalyst sample was degassed in a $N_2$/He mixture at 220 $^{o}$C for 4 h. X-ray photoelectron spectroscopy (XPS) analysis was performed on a Thermo Scientific Escalab 250Xi instrument, using monochromatic Al kα radiation (hν=1486.6 eV) operating at an accelerating power of 15 kW. Before the measurement, the sample was outgassed at room temperature in a UHV chamber (<5 ×$10^{-7}$ Pa). The sample charging effects were compensated by calibrating all binding energies (BE) with the adventitious C 1s peak at 284.6 eV. This reference gave BE values with an accuracy at ±0.1 eV.

Temperature-programmed desorption of ammonia ($NH_3$-TPD) experiments were performed to determine the surface acidity of catalysts, which were carried out on a

fixed-bed continuous flow microreactor equipped with a quadrupole mass spectrometer (QGA, Hidden, UK). Prior to each measurement, about 0.15 g sample was first pretreated in highly purified Ar flow (40 mL/min) at 400 $^{o}$C for 30 min. Then the reactor was cooled to 80 $^{o}$C and the sample was kept under 1% $NH_3$/Ar flow (40 ml/min) for about 2 h. The catalyst was then purged in Ar to remove gaseous and weakly adsorbed (physisorbed) $NH_3$, until achieving a constant level of a signal. Then desorption was started from 80 to 650 $^{o}$C with a linear heating rate of 2 $^{o}$C/min in a flow of Ar (40 ml/min).

Temperature-programmed reduction ($H_2$-TPR) experiments were carried out on a multifunction chemisorption analyzer (PCA-1200, Builder) with a quartz U-tube reactor, detected by a thermal conductivity detector (TCD). For each test, about 0.15 g sample was utilized. Before switching to the $H_2$-Ar stream, the sample was pretreated in Ar stream (40 mL/min) at 200 $^{o}$C for 30 min, and then cooled to 50 $^{o}$C. The sample was heated from 50 to 650 $^{o}$C with a ramping rate of 10 $^{o}$C/min under 5% $H_2$/Ar mixture flow (30 mL/min).

### 2.4 Catalytic activity tests

The $NH_3$-SCR catalytic activity tests of synthesized catalysts were carried out at atmospheric pressure in a fixed-bed stainless steel reactor with an internal diameter of 10 mm. The stainless steel reactor was installed in a vertical split-tube furnace. For each test, 0.15 g catalyst was charged. After the reactor was heated up to the desired reaction temperature, the inlet gas containing 500 ppm $NO_x$, 500 ppm $NH_3$, 5% $O_2$, and balance Ar was fed to the reactor with a flow rate of 200 mL/min. Afterwards, to determine the impact of $SO_2$ on the activity, the catalysts were studied by introducing 100 ppm $SO_2$ to the inlet gas (500 ppm $NO_x$, 500 ppm $NH_3$, 5% $O_2$, 100 ppm $SO_2$, balance Ar). All

the gas flows were controlled independently by mass flow controllers (Brooks Instruments). The $NO_x$ concentrations in the inlet and outlet gases were continuously analyzed using an on-line $NO_x$ analyzer (Thermo Scientific 42i-HL, USA). The $NO_x$ conversion at steady state was calculated using the follow equation (1). The deactivated catalysts were regenerated by heating the samples in air at a heating rate of 5 ºC/min to 400 ºC and held at this temperature 1 h purging with air.

$$NOx \text{ conversion} = \left(1 - \frac{NOx(out)}{NOx(in)}\right) \times 100\% \quad (1)$$

## 3. Results and discussion

### 3.1 Characterization of $Cu_yMn_zAl_{1-z}$-$CO_3$ LDHs

Fig. 1(a) shows the XRD patterns of synthesized $Cu_yMn_zAl_{1-z}$-$CO_3$ LDHs precursors with different Cu/(Mn+Al) molar ratios of 1, 2, 3, or 4 and Mn/Al molar ratio of 1. All samples presented the characteristic diffraction peaks of layered double hydroxide structure without any impurity phases, suggesting the complete incorporation of transition metals Mn and Cu into the crystalline structure. Sharp and intense Bragg reflections at 2θ = 11.72º, 23.53º, 34.59º, 39.44º, and 46.86º, can be indexed to the (003), (006), (012), (015), and (018) planes of $Cu_yMn_zAl_{1-z}$-$CO_3$ LDHs unit cell, respectively. Comparing to the typical Mg-Al-$CO_3$ LDH (JCPDS: 41-1428), the diffraction peaks slightly shifted to higher angles. This phenomenon can be explained by the distortion of the copper sites, which is caused by the Jahn–Teller effect of $Cu^{2+}$ ($d^9$) as reported by previous work.[30]

In addition, the $Cu_yMn_zAl_{1-z}$-$CO_3$ LDHs derived mixed oxides $Cu_yMn_zAl_{1-z}O_x$ were also analyzed. Fig. 1(b) shows that the layered structure of all LDHs transformed into mixed oxides after being calcined at 400 ºC. In all samples, the diffraction peaks

can be ascribed to the formation of crystallized CuO (JCPDS: No. 45-0937). No manganese oxide related crystalline phases was found, which indicates that Mn was finely dispersed within the mixed oxides.

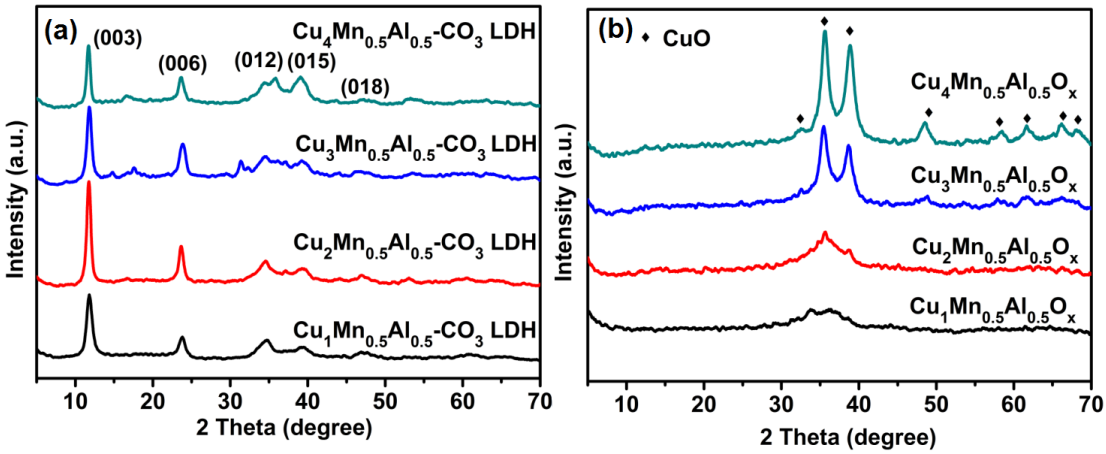


**Fig. 1.** XRD patterns of (a) $Cu_yMn_zAl_{1-z}$-$CO_3$ LDHs synthesized with different Cu/Al ratios, and (b) $Cu_yMn_zAl_{1-z}O_x$ calcined at 400 °C.

The physical properties of LDHs and the corresponding LDOs were evaluated by BET measurements, as shown in Table 1. As it can be seen, the SSA of $Cu_yMn_zAl_{1-z}$-$CO_3$ LDHs became higher with the increase in Cu/(Mn+Al) molar ratio, from 115.60 to 153.48–168.23 $m^2/g$. After calcination, the SSA of obtained mixed oxides were slightly decreased to the range of 96–136 $m^2/g$. Among all mixed oxides, $Cu_2Mn_{0.5}Al_{0.5}O_x$ showed the highest SSA, which is favorable for improving the SCR activity at certain extent. It is well known that higher SSA could provide more available active sites on the catalyst surface for reactants to participate reactions.[31, 32] The morphology of synthesized $Cu_yMn_zAl_{1-z}$-$CO_3$ LDHs were studied using FE-SEM and TEM analyses. Fig. 2 revealed that the $Cu_2Mn_{0.5}Al_{0.5}$-$CO_3$ LDH possesses "flower-like" hierarchical morphology with typical well-defined nanoplatelets. Similar morphology has been reported by Gennequin et al. for Mg–Al LDH.[33]

**Table 1.** Specific surface area, pore size, and pore volume of $Cu_yMn_zAl_{1-z}$-$CO_3$ LDHs and the corresponding $Cu_yMn_zAl_{1-z}O_x$ LDOs.

| Samples | BET SSA ($m^2/g$) | BJH Pore size (Å) | BJH pore volume ($cm^3/g$) |
|---|---|---|---|
| $Cu_1Mn_{0.5}Al_{0.5}CO_3$ LDH | 115.60 | 142.4 | 0.823142 |
| $Cu_2Mn_{0.5}Al_{0.5}CO_3$ LDH | 168.23 | 124.2 | 1.044717 |
| $Cu_3Mn_{0.5}Al_{0.5}CO_3$ LDH | 153.48 | 112.6 | 0.863760 |
| $Cu_4Mn_{0.5}Al_{0.5}CO_3$ LDH | 157.94 | 122.0 | 0.963069 |
| $Cu_1Mn_{0.5}Al_{0.5}O_x$ LDO | 133.26 | 114.1 | 0.760285 |
| $Cu_2Mn_{0.5}Al_{0.5}O_x$ LDO | 136.45 | 150.9 | 1.029414 |
| $Cu_3Mn_{0.5}Al_{0.5}O_x$ LDO | 110.40 | 123.9 | 0.684070 |
| $Cu_4Mn_{0.5}Al_{0.5}O_x$ LDO | 96.20 | 116.2 | 0.558993 |

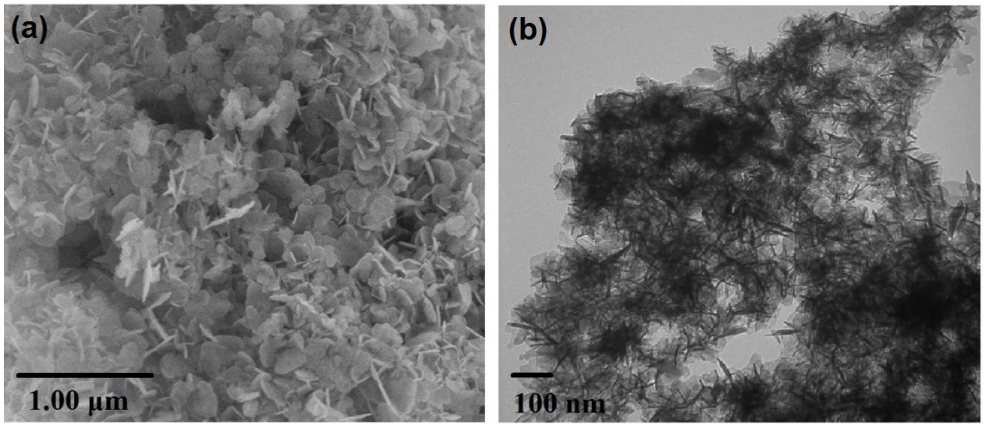


**Fig. 2.** (a) SEM and (b) TEM images of $Cu_2Mn_{0.5}Al_{0.5}$-$CO_3$ LDH.

Fig. 3 shows the FT-IR spectra of $Cu_yMn_zAl_{1-z}$-$CO_3$ LDHs and the corresponding LDOs. For fresh LDHs, similar FT-IR spectra to Mg–Al hydrotalcite were observed.[33] A broad absorption band centered at 3357 $cm^{-1}$ is attributed to the stretching vibrations of –OH groups in the brucite-like layers, the lattice water and the interlayer water molecules. The vibration of angular deformation of $H_2O$ molecules is observed at 1557 $cm^{-1}$. The absorption band at 1364 $cm^{-1}$ in the spectra can be related to the vibrations of carbonate ions. Finally, the absorption bands around 838 and 570 $cm^{-1}$ are attributed to the vibrations of the M–O (M–OH, M–O–M or O–M–O). Both XRD and FTIR data

confirmed the successful synthesis of $Cu_yMn_zAl_{1-z}$-$CO_3$ LDHs with different Cu/(Mn+Al) molar ratios.

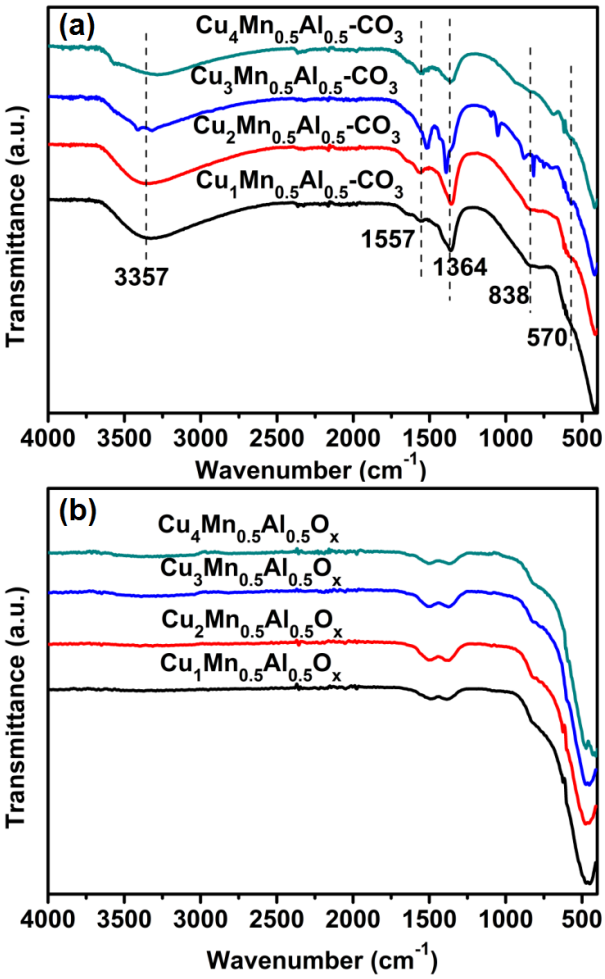


**Fig. 3.** FTIR spectra of (a) $Cu_yMn_zAl_{1-z}$-$CO_3$ LDHs with different Cu/(Mn+Al) ratios, and (b) $Cu_yMn_{0.5}Al_{0.5}O_x$ LDOs with different Cu/(Mn+Al) ratios obtained by calcining at 400 °C.

### 3.2 SCR activity of $Cu_yMn_zAl_{1-z}O_x$ mixed oxide catalysts

For the Mn-based SCR catalysts, it is apparent that the ratios of Cu/(Mn+Al) and Mn/Al will have a significant effect on the activity. Therefore, a series of $Cu_yMn_zAl_{1-z}O_x$ mixed oxides was studied for the SCR of $NO_x$. Fig. 4 shows the influences of Cu/(Mn+Al) ratio (1, 2, 3, and 4) and $Mn^{3+}/Al^{3+}$ ratio (1:3, 1:1, and 3:1) on the activity of $Cu_yMn_zAl_{1-z}O_x$ mixed oxide catalysts in the reaction temperature range of 100–250 °C. Initially, we

optimized the $M^{2+}/M^{3+}$ molar ratio of $CuMn_{0.5}Al_{0.5}O_x$ by changing the Cu/(Mn+Al) to be 1, 2, 3, and 4. The $NO_x$ conversion at 150 $^oC$ first increased with the increase in Cu/(Mn+Al) ratio from 1 to 2, and then started to decrease when the Cu/(Mn+Al) ratio from 3 to 4. Under all same testing conditions, the $NO_x$ conversion of $Cu_1Mn_{0.5}Al_{0.5}O_x$, $Cu_2Mn_{0.5}Al_{0.5}O_x$, $Cu_3Mn_{0.5}Al_{0.5}O_x$, and $Cu_4Mn_{0.5}Al_{0.5}O_x$ catalyst at 150 $^oC$ were 74.3%, 91.2%, 87.5%, and 76.9%, respectively. This data clearly indicated that the Cu/(Mn+Al) molar ratio has a strong influence on the SCR activity of catalysts, and the composition of $Cu_2Mn_{0.5}Al_{0.5}O_x$ exhibited the highest $NO_x$ conversion of 91.2% at 150 $^oC$ (Fig. 4(a)).

After revealing the best $M^{2+}/M^{3+}$ ratio, the impact of $Mn^{3+}/Al^{3+}$ molar ratio (1:3, 1:1, and 3:1) was also studied, as shown in Fig. 4(b). At all temperatures ranging form 100 to 250 $^oC$, the $NO_x$ conversions all increased with the increase of $Mn^{3+}/Al^{3+}$ molar ratio from 1:3 to 1:1. However, further increasing the $Mn^{3+}/Al^{3+}$ molar ratio from 1:1 to 3:1 resulted in a decline in $NO_x$ conversion. For instance, at 100, 150, 200, and 250 $^oC$, the $NO_x$ conversions were decreased from 51.6%, 91.2%, 83.6%, and 70.4% to 35.2%, 85.7%, 82.4%, and 67%, respectively. Previous researches have also demonstrated that there is always an optimal loading for the active component. When the loading of the active component was increased beyond a certain value, sintering would take place on the surface of catalysts and result in the formation of crystallization, thereby lowering the activity.[34, 35] In summary, the $Cu_2Mn_{0.5}Al_{0.5}O_x$ catalyst showed the best SCR catalytic performance with Cu/(Mn+Al) molar ratio being 2:1, and the $Mn^{3+}/Al^{3+}$ molar ratio being 1:1, with a $NO_x$ conversion of 91.2% at 150 $^oC$.

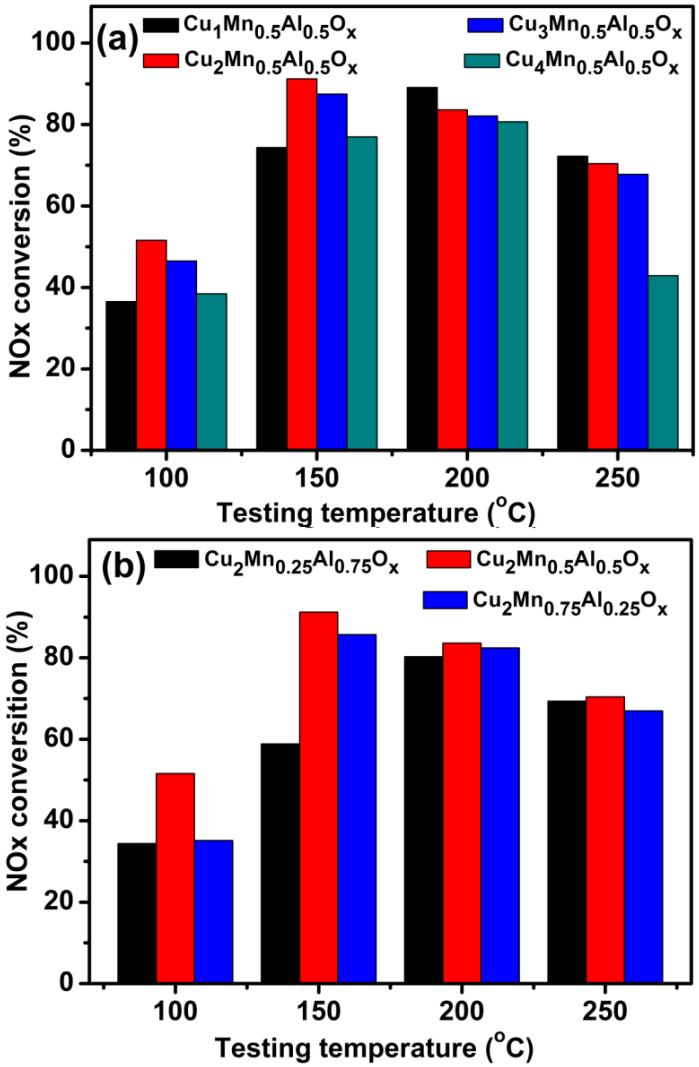


**Fig. 4.** The influence of (a) Cu/(Mn+Al) ratio (1, 2, 3, and 4), and (b) $Mn^{3+}/Al^{3+}$ ratio (1:3, 1:1, and 3:1) on the activity of $Cu_yMn_zAl_{1-z}O_x$ mixed oxide catalysts. Calcination temperature = 400 °C, and operating temperature =100, 150, 200, and 250 °C. Reaction conditions: $[NO_x] = [NH_3]$ = 500 ppm, $[O_2]$ = 5%, balance Ar, total flow rate = 200 mL/min, catalyst 0.15 g.

### 3.3 Comparison of $Cu_2Mn_{0.5}Al_{0.5}O_x$, $Cu_2AlO_x$, Cu-Mn/γ-$Al_2O_3$, and Mn/γ-$Al_2O_3$ catalysts

Previously, there are a few reports on conventional supported $Mn/Al_2O_3$ as $NH_3$-SCR catalyst. For instance, Singoredjo et al.[10] and Kijlstra et al.[36] studied the catalytic

activity and $SO_2$ resistance of $MnO_x/Al_2O_3$ catalysts and found that they are very sensitive to $SO_2$. In addition, Kang et al.[20] investigated Cu-Mn mixed oxides catalyst, with which the deactivation phenomenon due to the presence of water vapor and $SO_2$ was also observed. In the following section, a comparative study on $Cu_2Mn_{0.5}Al_{0.5}O_x$, $Cu_2AlO_x$, Cu-Mn/γ-$Al_2O_3$, and Mn/γ-$Al_2O_3$ was performed. Fig. 5(a) shows the $NO_x$ conversions of these four catalysts as a function of temperature for $NH_3$-SCR. For $Cu_2Mn_{0.5}Al_{0.5}O_x$ and $Cu_2AlO_x$ samples, both of them exhibited better $NO_x$ conversion compared with the supported catalysts of Mn/γ-$Al_2O_3$ and Cu-Mn/γ-$Al_2O_3$ at 100–250 $^oC$. For $Cu_2Mn_{0.5}Al_{0.5}O_x$, the highest $NO_x$ conversion was achieved at 200 $^oC$, which was 91.2%. While the maximal $NO_x$ conversions for $Cu_2AlO_x$, Cu-Mn/γ-$Al_2O_3$, and Mn/γ-$Al_2O_3$ catalysts were achieved at 200 $^oC$, which are only 84.2%, 82.6%, and 67.2%, respectively. It is apparent that the $Cu_2Mn_{0.5}Al_{0.5}O_x$ catalyst possesses much better SCR performance than the other three catalysts, particularly in the temperature range of 150–200 $^oC$. In addition, the optimal operating temperature of $Cu_2Mn_{0.5}Al_{0.5}O_x$ (150 $^oC$) was also lower than that of other samples (200 $^oC$). In all, it can be concluded that our newly designed catalyst $Cu_2Mn_{0.5}Al_{0.5}O_x$ possesses much better low-temperature SCR performance than other catalysts including $Cu_2AlO_x$, Cu-Mn/γ-$Al_2O_3$, and Mn/γ-$Al_2O_3$ catalysts.

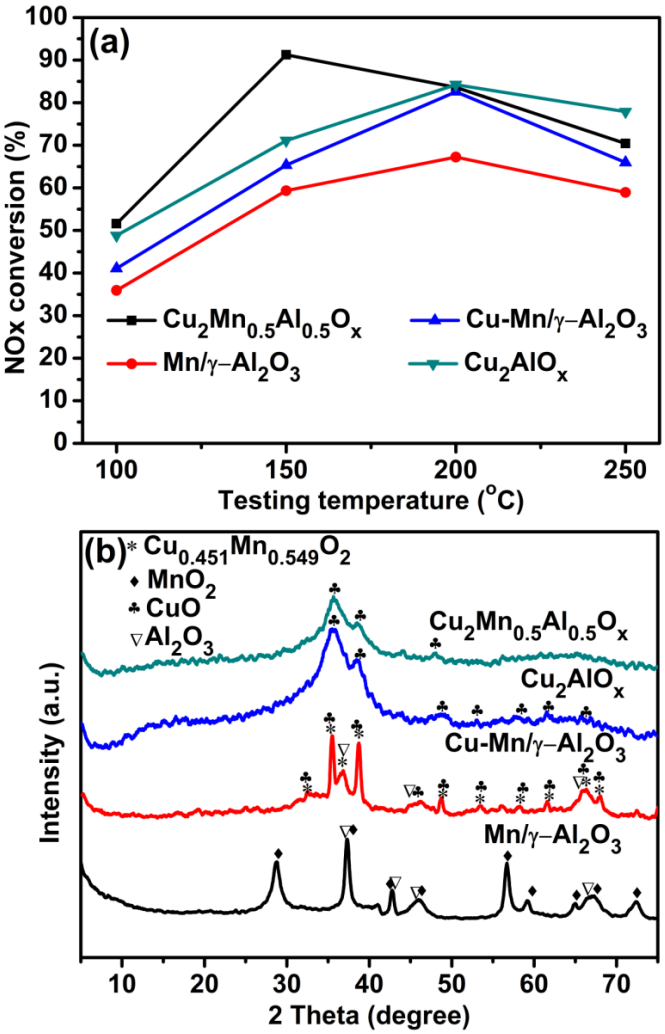


**Fig. 5.** (a) The $NO_x$ conversion over $Cu_2Mn_{0.5}Al_{0.5}O_x$, $Cu_2AlO_x$, Cu-Mn/γ-$Al_2O_3$, and Mn/γ-$Al_2O_3$ catalysts as a function of temperature. (b) The XRD patterns of $Cu_2Mn_{0.5}Al_{0.5}O_x$, $Cu_2AlO_x$, Cu-Mn/γ-$Al_2O_3$, and Mn/γ-$Al_2O_3$ calcined at 400 °C. Operating temperature =100, 150, 200, and 250 °C. Reaction conditions: [$NO_x$] = [$NH_3$] = 500 ppm, [$O_2$] = 5%, balance Ar, total flow rate = 200 mL/min, catalyst 0.15 g.

In order to understand why the $Cu_2Mn_{0.5}Al_{0.5}O_x$ catalyst has better activity at low temperature than other catalysts, the XRD patterns of these catalysts were examined after being calcined at 400 °C, as shown in Fig 5(b). For Mn/γ-$Al_2O_3$, crystallized $MnO_2$ (JCPDS: No. 24-0735) and $Al_2O_3$ (JCPDS: No. 04-0880) were observed. While after introducing Cu, a mixture of oxides and spinel were detected for Cu-Mn/γ-$Al_2O_3$,

including CuO (JCPDS: No. 45-0937), $Al_2O_3$ (JCPDS: No. 04-0880) and $Cu_{0.451}Mn_{0.549}O_2$ (JCPDS: No. 41-0184) spinel phases. For $Cu_2Mn_{0.5}Al_{0.5}O_x$ and $Cu_2AlO_x$ samples, only CuO phase was observed. No crystalline phase ascribed to manganese oxide can be found. It suggests that manganese oxide is finely dispersed as a non-crystalline phase or the particle size is smaller than the detection limit of XRD analysis. Moreover, aluminum oxide was not observed neither because it was in an amorphous state at this calcination temperature.[37] This may be ascribed to that the transition metal Cu has positive effect on the activity of catalysts and could reduce the crystallinity of manganese oxide and weaken the sintering in catalysts, which is in accordance with previous study. [38, 39]

The chemical composition and the oxidation state of manganese and copper in different catalysts were examined using XPS analyses. Fig. 6 shows the XPS spectra of Mn 2p, Cu 2p and O 1s of $Cu_2Mn_{0.5}Al_{0.5}O_x$, $Cu_2AlO_x$, Cu-Mn/γ-$Al_2O_3$, and Mn/γ-$Al_2O_3$ catalysts. The surface components of these samples were summarized in Table 2. The Mn 2p XPS profile indicated that $MnO_x$ existed in the form of a mixed-valence manganese system on catalysts surface. Two main peaks corresponding to Mn 2p1/2 and Mn 2p3/2 were observed at around 632−658 eV for all samples. By performing peak-fitting deconvolutions, the Mn 2p3/2 of mixed-valence manganese system can be divided into two characteristic peaks, which can be attributed to $Mn^{4+}$ (643.2 ± 0.2 eV) and $Mn^{3+}$ (642.0 ± 0.2 eV), respectively.[40] The SCR of $NO_x$ over the pure manganese oxides at the low temperature was investigated by Kapteijn et al.[41] They found that the De-$NO_x$ efficiency decreased in the order of $MnO_2$ > $Mn_5O_8$ > $Mn_2O_3$ > $Mn_3O_4$. The relative concentrations of $Mn^{4+}$ in this research follows the order of $Cu_2Mn_{0.5}Al_{0.5}O_x$ > Cu-Mn/γ-$Al_2O_3$ > Mn/γ-$Al_2O_3$. Previous studies have demonstrated that the higher oxidation state of manganese species ($Mn^{4+}$) was preferable for the redox properties of

manganese-based catalysts.[42, 43] Thus, the high concentration of $Mn^{4+}$ in $Cu_2Mn_{0.5}Al_{0.5}O_x$ catalyst is favorable for its excellent low-temperature SCR activity.

**Table 2.** The surface components of $Cu_2Mn_{0.5}Al_{0.5}O_x$, $Cu_2AlO_x$, Cu-Mn/γ-$Al_2O_3$, and Mn/γ-$Al_2O_3$ catalysts obtained by XPS analyses.

| Catalysts | Mn (at.%) | Cu (at.%) | O (at.%) | $Mn^{4+}$ (%) | $Cu^{2+}$ (%) | $O_\beta$ (%) |
|---|---|---|---|---|---|---|
| $Cu_2Mn_{0.5}Al_{0.5}O_x$ | 9.1 | 13.15 | 32.74 | 67.7 | 93.5 | 65.3 |
| $Cu_2AlO_x$ | - | 13.94 | 32.44 | - | 91.3 | 61.7 |
| Cu-Mn/γ-$Al_2O_3$ | 1.63 | 1.8 | 56.8 | 66.8 | 86.3 | 56.9 |
| Mn/γ-$Al_2O_3$ | 0.88 | - | 57.74 | 40.2 | - | 37.3 |

Fig. 6(b) presents the Cu 2p XPS spectra of $Cu_2Mn_{0.5}Al_{0.5}O_x$, $Cu_2AlO_x$ and Cu-Mn/γ-$Al_2O_3$ catalysts. The satellite peaks at 938.0–945.0 eV and 960.0–965.0 eV, and the intense and broad photoelectron peaks at about 934 eV (Cu 2p3/2) and 955.0 eV (Cu 2p1/2) were observed for all the catalysts. The relative intensity of $Cu^{2+}$ of $Cu_2Mn_{0.5}Al_{0.5}O_x$ (93.5%) is higher than that of $Cu_2AlO_x$ (91.3%) and Cu-Mn/γ-$Al_2O_3$ (86.3%), which are favorable for the high $NO_x$ conversion activity.

Fig. 6(c) shows the O 1s XPS spectra of $Cu_2Mn_{0.5}Al_{0.5}O_x$, $Cu_2AlO_x$, Cu-Mn/γ-$Al_2O_3$, and Mn/γ-$Al_2O_3$ catalysts. The O 1s spectra of all catalysts can be fitted into two peaks. The peak at lower binding energy (528.7–530.9 eV) corresponds to lattice oxygen ($O_\alpha$), whereas the one at higher binding energy (531.4–532.5 eV) is related to the surface adsorbed oxygen ($O_\beta$).[44] It is worth to notice that the relative concentration ratio of $O_\beta$ increased and reached the maximum value with $Cu_2Mn_{0.5}Al_{0.5}O_x$ catalyst, as shown in Table. 2. This implies that the synthesis of $Cu_2Mn_{0.5}Al_{0.5}O_x$ mixed oxide from LDH can resulted in more surface oxygen vacancies. It has been reported that the surface adsorbed oxygen ($O_\beta$) plays a key role in the SCR reaction due to its higher mobility.[45, 46] As reported by Liu et al. [47], the $O_\beta$ can promote the oxidation of NO into

$NO_2$, and consequently facilitate the "fast SCR" reaction. For the Mn/γ-$Al_2O_3$ and Cu-Mn/γ-$Al_2O_3$ catalysts, their $O_\beta$ amounts are notably lower than that of $Cu_2Mn_{0.5}Al_{0.5}O_x$ and $Cu_2AlO_x$ samples. Based on the XPS analysis, it can be concluded that the high concentrations of $Mn^{4+}$, $Cu^{2+}$ and $O_\beta$ should also be partly responsible for the good $NO_x$ conversion of $Cu_2Mn_{0.5}Al_{0.5}O_x$ catalyst.

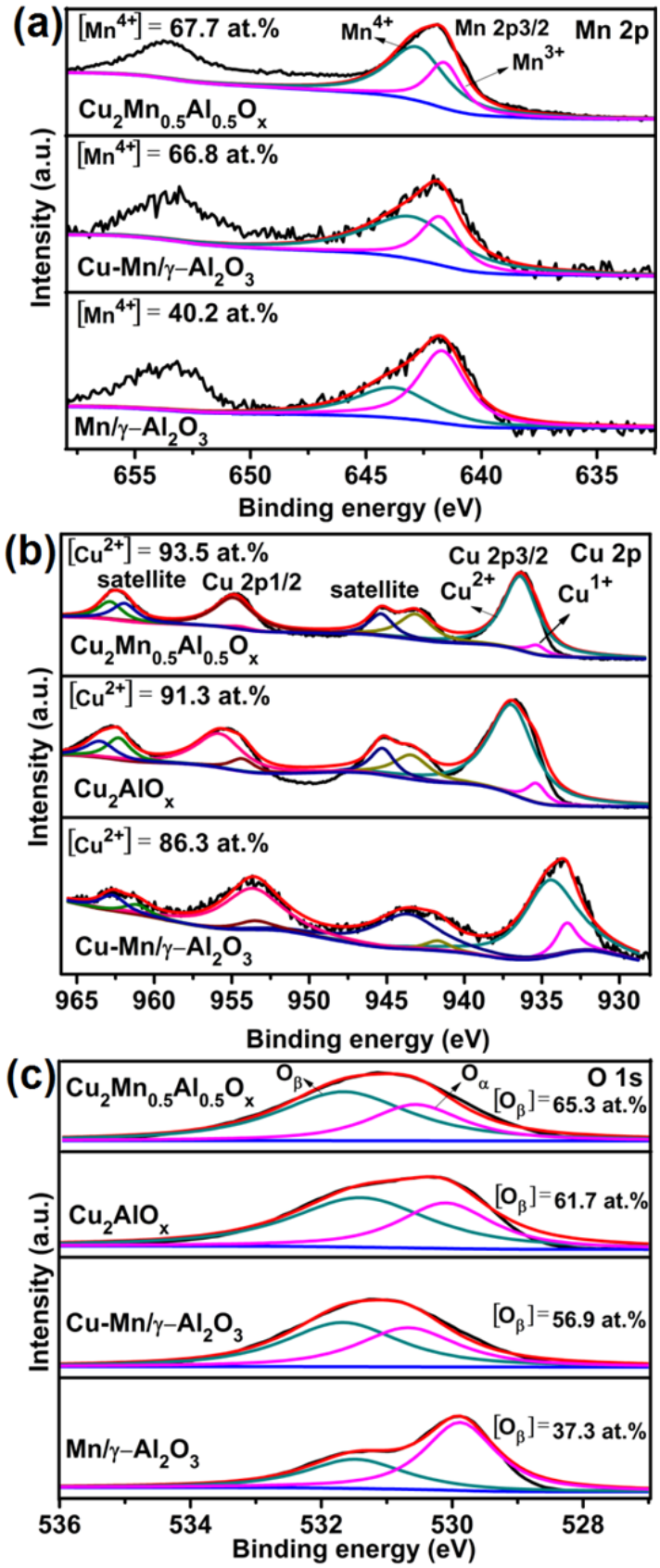


**Fig. 6.** XPS results of (a) Mn 2p, (b) Cu 2p, and (c) O 1s over $Cu_2Mn_{0.5}Al_{0.5}O_x$, $Cu_2AlO_x$, Cu-Mn/γ-$Al_2O_3$, and Mn/γ-$Al_2O_3$ catalysts.

The amount and strength of surface acidity of catalysts were probed by $NH_3$-TPD analysis. As shown in Fig. 7(a), $NH_3$ desorption is observed over a wide temperature range, due to the variability of adsorbed $NH_3$ species with different thermal stabilities. Desorption peaks of all samples located at about 150 $^oC$. The amounts of desorbed $NH_3$ (surface acidity) over $Cu_2Mn_{0.5}Al_{0.5}O_x$, $Cu_2AlO_x$, Cu-Mn/γ-$Al_2O_3$, and Mn/γ-$Al_2O_3$ were compared by integrating the $NH_3$-TPD curves, and the area ratio among is approximately 2.58:1.24:1.16:1. This suggests that surface acidity of $Cu_2Mn_{0.5}Al_{0.5}O_x$ and $Cu_2AlO_x$ is much higher than that of Cu-Mn/γ-$Al_2O_3$ and Mn/γ-$Al_2O_3$. The reaction mechanism of $NH_3$-SCR in the presence of excess oxygen has been investigated extensively and the surface acidity is considered to be closely related to the catalytic activity.[48]

The redox behaviors of catalysts were studied using $H_2$-TPR analysis, as shown in Fig. 7(b). Two reduction peaks for Mn/γ-$Al_2O_3$ were observed, which can be ascribed to the reduction of $MnO_x$ species. In addition, the low-temperature reduction peak area of Cu-Mn/γ-$Al_2O_3$ and $Cu_2Mn_{0.5}Al_{0.5}O_x$ is significantly larger than that of Mn/γ-$Al_2O_3$. The enhancement maybe due to the synergistic effect between the copper and manganese oxide, which can create oxygen defects, and structural distortion. Thus, the synthesized $Cu_2Mn_{0.5}Al_{0.5}O_x$ mixed oxide from LDH possesses higher reducibility of $MnO_x$, implying the mobility of surface oxygen was enhanced and beneficial for the SCR reaction.[49, 50]

Compared with Mn/γ-$Al_2O_3$, the stepwise reduction peak of $MnO_x$ for $Cu_2Mn_{0.5}Al_{0.5}O_x$ is broadened greatly due to the good dispersion of Mn species and its interaction with Cu. The broad reduction peak (150-500 $^oC$) of $Cu_2Mn_{0.5}Al_{0.5}O_x$ catalyst could be assigned to the stepwise reduction of $MnO_x$, i.e., $MnO_2 \rightarrow Mn_2O_3 \rightarrow Mn_3O_4$

→ MnO, overlapped with the reduction of surface $Cu^{2+}$.[20] Moreover, the reduction peak area of $Cu_2Mn_{0.5}Al_{0.5}O_x$ is also larger than that of $Cu_2AlO_x$.

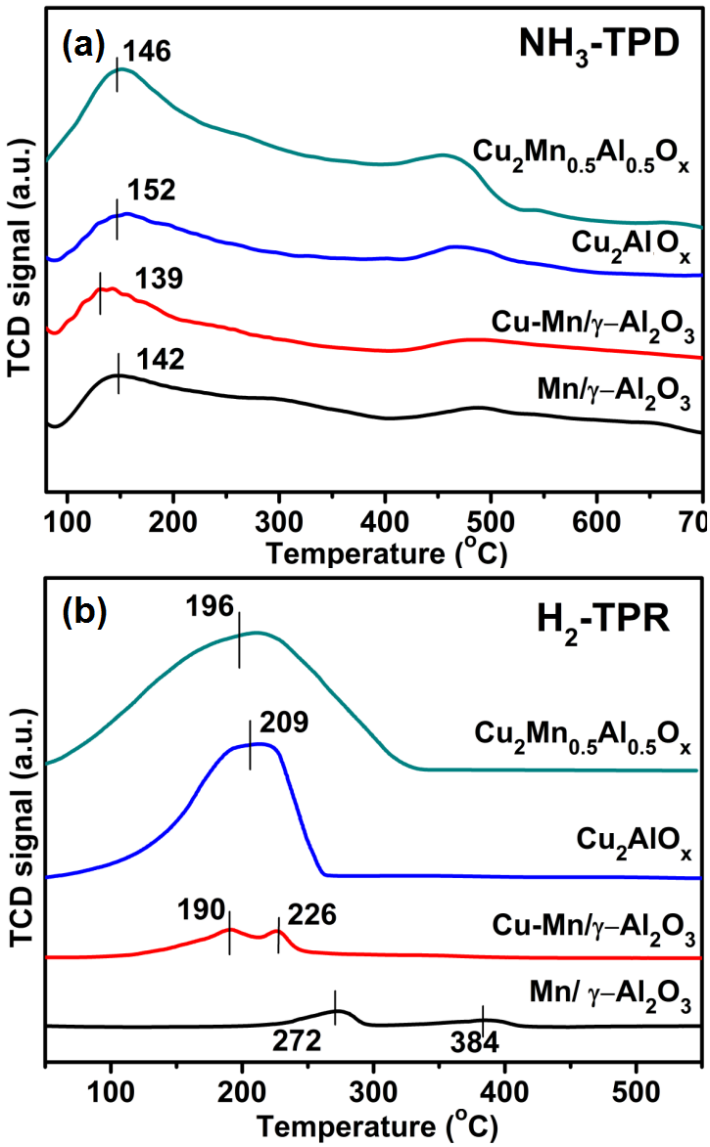


**Fig. 7.** (a) $NH_3$-TPD profiles over the $Cu_2Mn_{0.5}Al_{0.5}O_x$, $Cu_2AlO_x$, Cu-Mn/γ-$Al_2O_3$, and Mn/γ-$Al_2O_3$ catalysts, (b) $H_2$-TPR profiles over the $Cu_2Mn_{0.5}Al_{0.5}O_x$, $Cu_2AlO_x$, Cu-Mn/γ-$Al_2O_3$, and Mn/γ-$Al_2O_3$ catalysts.

### 3.4 $SO_2$ and $H_2O$ poisoning of catalysts

In practical working conditions, the effluent gases always contain a small amount of $SO_2$ and water vapor, which is a challenge for $NH_3$-SCR catalysts, especially for Mn-

based catalysts.[20] At first, $SO_2$ could react with $NH_3$ to form $(NH_4)_2SO_3$ and $NH_4HSO_4$, which did not decompose below 200 $^oC$ and finally deposited on catalyst surface, causing pore plugging of catalysts. In addition, $SO_2$ may react with the active components, which cause inactivation for the $NH_3$-SCR reaction. Thus, the influence of $SO_2$ on catalytic performance must be considered for $NH_3$-SCR catalysts. Fig. 8(a) shows the effects of 100 ppm $SO_2$ on the SCR activities of all four catalysts at 150 $^oC$. After a small and temporary increase of the $NO_x$ conversion, the catalytic activity decreased with time. It indicated that the effect of $SO_2$ on the activity of catalysts at low temperature was inhibited for a short time, but eventually resulted in catalyst poisoning. The decreased activity may be caused by tightly absorbed $SO_2$, formed sulfates and other species on the surface occupying the active sites (such as $MnO_x$, CuO), which consequently decreased the SCR activity. With 100 ppm $SO_2$ was added to the system, the $NO_x$ conversion for $Cu_2Mn_{0.5}Al_{0.5}O_x$, $Cu_2AlO_x$, Cu-Mn/γ-$Al_2O_3$, and Mn/γ-$Al_2O_3$ catalysts was 64.9%, 57.2%, 49.3% and 45.5% after 1 h, and then decreased to 49.5%, 43.1%, 34.6% and 20.2% after 3h at 150 $^oC$, respectively. It can be concluded that the catalysts prepared from LDH precursors had relatively better $SO_2$ resistance. The $SO_2$ poisoning mechanism for $Cu_2Mn_{0.5}Al_{0.5}O_x$ catalyst was investigated using FT-IR analyses. Fig. 8(b) shows the FT-IR spectra of fresh and pre-sulfated $Cu_2Mn_{0.5}Al_{0.5}O_x$ catalyst. Two new peaks located at 1128 and 1051 $cm^{-1}$ were observed with the pre-sulfated $Cu_2Mn_{0.5}Al_{0.5}O_x$, which could be assigned to the $SO_4^{2-}$ species on acid sites. [51]

In order to investigate the effect of $SO_2$ on the redox properties of catalysts, the fresh and pre-sulfated catalysts were characterized by $H_2$-TPR. As shown in Fig. 8(c, d), compared with fresh catalysts, the reduction peaks of pre-sulfated catalysts moved to higher temperatures. It is well recognized that the reduction peak temperature is an indication of reducibility, and lower reduction temperature means stronger

reducibility.[51] In addition, the reduction peak area of all the catalysts decreased, which indicated that $SO_2$ had negative effect on the reducibility of catalysts. For Mn/γ-$Al_2O_3$ catalyst, the two low-temperature peaks located at 272 and 384 °C greatly moved to 301 and 406 °C. However, after adding Cu to Mn/γ-$Al_2O_3$ catalyst, the reduction peak temperatures of Cu-Mn/γ-$Al_2O_3$ only slightly increased, from 190 and 226 °C to 219 and 255 °C. These data demonstrated that the addition of Cu can promote the $SO_2$ resistance of Mn-based SCR catalyst. For the $Cu_2Mn_{0.5}Al_{0.5}O_x$ and $Cu_2AlO_x$ catalysts obtained from LDHs precursors, the reduction peak temperatures were still very low even after $SO_2$ presulfation, which only slightly increased from 196 and 209 °C to 221 and 230 °C, respectively. Comparing to $Cu_2AlO_x$, the redox peak somehow stronger and the peak temperature was slightly lower for $Cu_2Mn_{0.5}Al_{0.5}O_x$. This might be the reason why $Cu_2Mn_{0.5}Al_{0.5}O_x$ catalyst has the best $SO_2$ resistance among all studied catalysts.

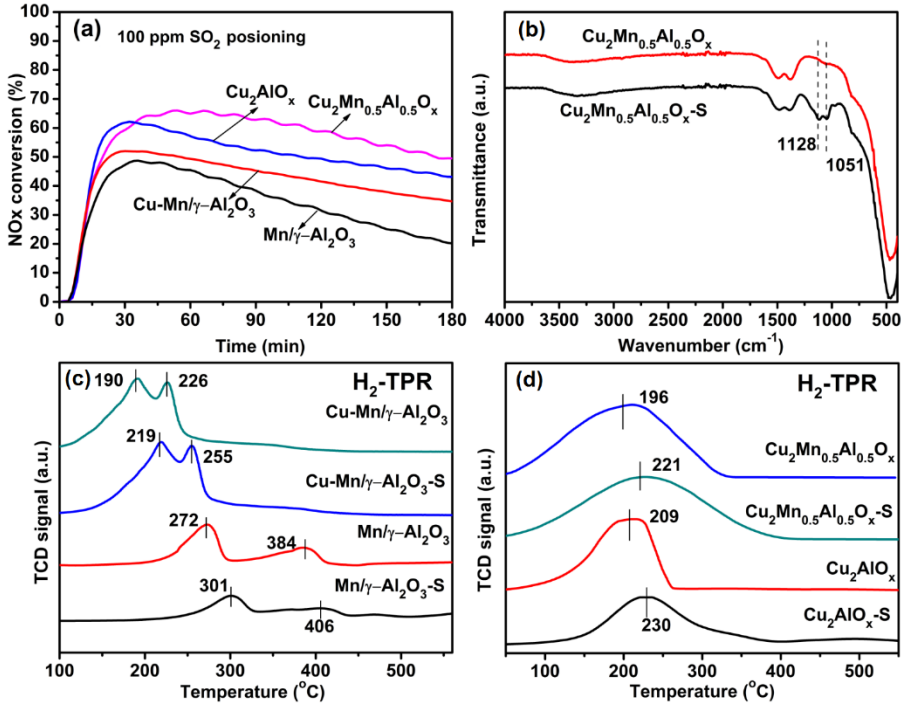


**Fig. 8.** (a) SCR activities of $Cu_2Mn_{0.5}Al_{0.5}O_x$, $Cu_2AlO_x$, Cu-Mn/γ-$Al_2O_3$, and Mn/γ-$Al_2O_3$ catalysts in the presence of $SO_2$, (b) FTIR spectra of $Cu_2Mn_{0.5}Al_{0.5}O_x$ and pre-

sulfated $Cu_2Mn_{0.5}Al_{0.5}O_x$, (c) $H_2$-TPR of fresh and pre-sulfated Cu-Mn/γ-$Al_2O_3$, and Mn/γ-$Al_2O_3$ catalysts, and (d) $H_2$-TPR of fresh and pre-sulfated $Cu_2Mn_{0.5}Al_{0.5}O_x$, and $Cu_2AlO_x$ catalysts. Reaction conditions: [$NO_x$] = [$NH_3$] = 500 ppm, [$O_2$] = 5%, [$SO_2$] = 100 ppm, balance Ar, total flow rate = 200 mL/min, catalyst 0.15 g.

In addition, the SSA of fresh and deactivated catalysts are summarized in Table 3. The SSA for fresh $Cu_2Mn_{0.5}Al_{0.5}O_x$, $Cu_2AlO_x$, Cu-Mn/γ-$Al_2O_3$, and Mn/γ-$Al_2O_3$ was 136.4, 117.8, 144.6, and 135.6 $m^2/g$, respectively. After the sulfate species were formed and deposited on catalysts surface, the SSA of all sulfated $Cu_2Mn_{0.5}Al_{0.5}O_x$, $Cu_2AlO_x$, Cu-Mn/γ-$Al_2O_3$, and Mn/γ-$Al_2O_3$ became 127.4, 105.2, 103.9, and 100.4 $m^2/g$, respectively. It is apparent that the SSA of all samples decreased for a certain degree, which may be one reason that explains the decrease in catalytic activity. However, it is apparent that the SSA decreases for $Cu_2Mn_{0.5}Al_{0.5}O_x$ was much smaller than other catalysts, only 9 $^oC$. In addition, the changes in pore size and pore volume of $Cu_2Mn_{0.5}Al_{0.5}O_x$ after $SO_2$ poisoning were also slight, which indicated that most of the sulfate species were deposited on the surface of catalysts, rather than in the micropores.[52] The BET analyses also confirmed that the $Cu_2Mn_{0.5}Al_{0.5}O_x$ catalyst is much more $SO_2$ resistant than the other controlled catalysts.

**Table 3.** Specific surface area, pore size, and pore volume of fresh and sulfated $Cu_2Mn_{0.5}Al_{0.5}O_x$, $Cu_2AlO_x$, Cu-Mn/γ-$Al_2O_3$, and Mn/γ-$Al_2O_3$.

| Samples | BET SSA ($m^2/g$) | BJH Pore size (Å) | BJH pore volume ($cm^3/g$) |
|---|---|---|---|
| $Cu_2Mn_{0.5}Al_{0.5}O_x$ | 136.4 | 150.9 | 1.029414 |
| $Cu_2AlO_x$ | 117.8 | 124.9 | 0.735527 |
| Cu-Mn/γ-$Al_2O_3$ | 144.6 | 49.9 | 0.360984 |
| Mn/γ-$Al_2O_3$ | 135.6 | 54.9 | 0.371907 |
| $Cu_2Mn_{0.5}Al_{0.5}O_x$-S | 127.4 | 150.1 | 0.955845 |
| $Cu_2AlO_x$-S | 105.2 | 66.3 | 0.874491 |

| | | | |
|---|---|---|---|
| Cu-Mn/γ-$Al_2O_3$-S | 103.9 | 63.1 | 0.674379 |
| Mn/γ-$Al_2O_3$-S | 100.4 | 61.2 | 0.613279 |

The effect of $H_2O$ on the performance of catalysts was also tested. At 150 $^oC$, the $NO_x$ concentrations were recorded for 2 h, as shown in Fig. 9(a). In general, the existence of 5% $H_2O$ showed visible $NO_x$ conversion decreases at 150 $^oC$ for all catalysts. But $Cu_2Mn_{0.5}Al_{0.5}O_x$ was less influenced, with the $NO_x$ conversion remained as high as 78.18%. Meanwhile, the $NO_x$ conversions of $Cu_2AlO_x$, Cu-Mn/γ-$Al_2O_3$, and Mn/γ-$Al_2O_3$ catalysts were decreased to 63.64%, 46.02%, and 37.2% respectively. After stopping $H_2O$ from the feed gases, the $NO_x$ conversions can be restored to some extent, but still below the initial values, representing parts of the deactivation effect by $H_2O$ is irreversible. The hindering effect by $H_2O$ at low temperatures is mainly due to the competitive adsorption of $H_2O$ with the reactants at the same active sites. Overall, this data suggests that $Cu_2Mn_{0.5}Al_{0.5}O_x$ catalyst also possesses much better $H_2O$ resistance than the other catalysts studied in this work.

Fig. 9(b) compares the SCR activities of different catalysts in the presence of both $SO_2$ and $H_2O$ simultaneously. After adding 5% $H_2O$ and 100 ppm $SO_2$, the $NO_x$ conversions of all catalysts decreased to certain degree within 2 h at 150 $^oC$. Nevertheless, $Cu_2Mn_{0.5}Al_{0.5}O_x$ still showed the highest activity comparing to other three catalysts. The $NO_x$ conversions of $CuMn_{0.5}Al_{0.5}O_x$, $Cu_2Mn_{0.5}Al_{0.5}O_x$, $Cu_2AlO_x$, Cu-Mn/γ-$Al_2O_3$, and Mn/γ-$Al_2O_3$ were about 62.18%, 49.6%, 41.5%, and 31.3% respectively. Upon removing $H_2O$ and $SO_2$ from the feed gases, although the $NO_x$ conversions could not return to their previous levels, they all were increased obviously. Particularly for $Cu_2Mn_{0.5}Al_{0.5}O_x$, the $NO_x$ conversion was recovered from 62.18% to 80.7% after cutting down $H_2O$ and $SO_2$.

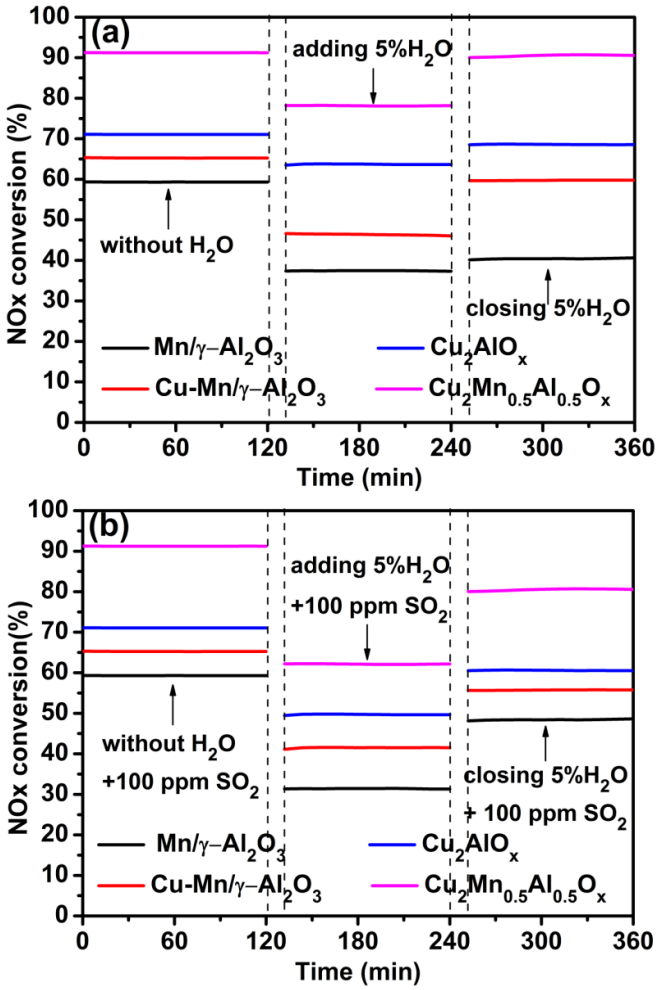


**Fig. 9.** (a) The effect of individual $H_2O$ and (b) the effect of $SO_2$ and $H_2O$ co-existence on the $NO_x$ conversions over $Cu_2Mn_{0.5}Al_{0.5}O_x$, $Cu_2AlO_x$, Cu-Mn/γ-$Al_2O_3$ and Mn/γ-$Al_2O_3$ catalysts at 150 °C. Reaction conditions: [$NO_x$] = [$NH_3$] = 500 ppm, [$O_2$] = 5%, [$H_2O$] = 5%, [$SO_2$] = 100 ppm, balance Ar, total flow rate = 200 mL/min, catalyst 0.15 g.

### 3.5 Regeneration of deactivated catalysts

Considering the fact that the deactivation of catalysts can not be completely prevented, the regenerability of deactivated catalysts is also very important. In this study, thermal regeneration was selected to recover the catalytic activity of all deactivated catalysts. The deactivated catalyst was a vulcanized catalyst obtained after the above 100 ppm

$SO_2$ sulfur resistance test. Fig. 10(a) shows the $NO_x$ conversion on the deactivated catalysts after thermal regeneration. The $NO_x$ conversion on fresh $Cu_2Mn_{0.5}Al_{0.5}O_x$, $Cu_2AlO_x$, Cu-Mn/γ-$Al_2O_3$ and Mn/γ-$Al_2O_3$ were about 91.2%, 71.1%, 65.3% and 59.3% at 150 ºC, respectively. With 100 ppm $SO_2$ was added to the system, the $NO_x$ conversion for $Cu_2Mn_{0.5}Al_{0.5}O_x$, $Cu_2AlO_x$, Cu-Mn/γ-$Al_2O_3$, and Mn/γ-$Al_2O_3$ catalysts was 34.2%, 28.3%, 22.4% and 8.1% after 12 h. After thermal regeneration, the catalytic activities of $Cu_2Mn_{0.5}Al_{0.5}O_x$, $Cu_2AlO_x$, Cu-Mn/γ-$Al_2O_3$ and Mn/γ-$Al_2O_3$ were recovered to 84.8%, 61.6%, 57.9, and 48.8%, respectively. In addition, the catalyst after the regeneration was also investigated using FT-IR analyses. Fig. 10(b) shows the FT-IR spectra of fresh, pre-sulfated, and regenerative $Cu_2Mn_{0.5}Al_{0.5}O_x$ catalyst. The peak belongs to $SO_4^{2-}$ species apparently disappear after regeneration. It is indicated that most of sulfate and nitrate species deposited on the deactivated catalyst could be removed by thermal regeneration. These results clearly indicated that $Cu_2Mn_{0.5}Al_{0.5}O_x$ has much better regenerability and greater potential for practical applications than $Cu_2AlO_x$, Cu-Mn/γ-$Al_2O_3$, and Mn/γ-$Al_2O_3$ catalysts.

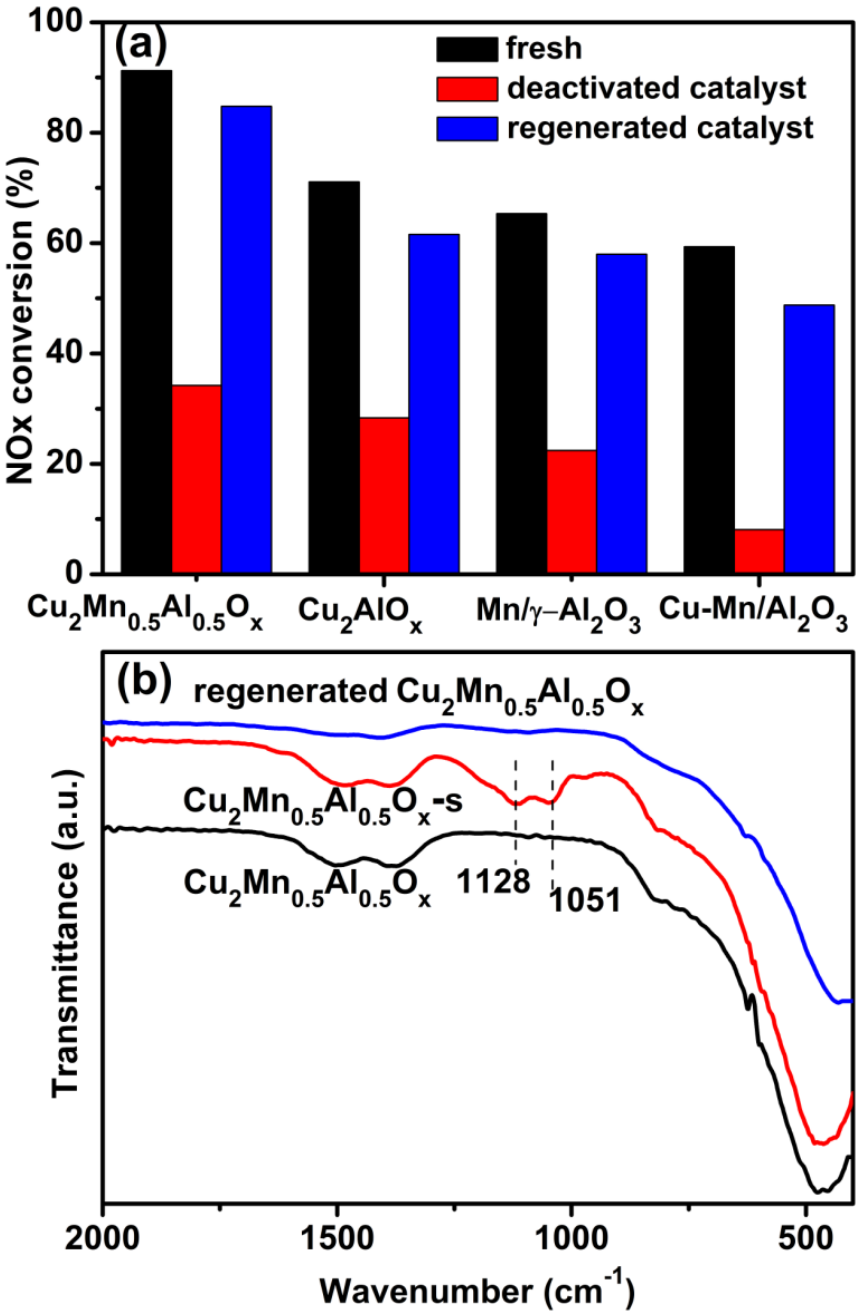


**Fig. 10.** (a) $NO_x$ conversions of fresh, deactivated and regenerated catalysts treated by thermal regeneration, and (b) FTIR spectra of $Cu_2Mn_{0.5}Al_{0.5}O_x$, pre-sulfated $Cu_2Mn_{0.5}Al_{0.5}O_x$, and regenerated $Cu_2Mn_{0.5}Al_{0.5}O_x$, Reaction conditions: $[NO_x]$ = $[NH_3]$ = 500 ppm, $[O_2]$ = 5%, balance Ar, total flow rate = 200 mL/min, catalyst 0.15 g.

## 4. Conclusions

Highly dispersed $Cu_2Mn_{0.5}Al_{0.5}O_x$ mixed oxide was synthesized from the corresponding $Cu_2Mn_{0.5}Al_{0.5}$-$CO_3$ LDH as an excellent low-temperature $NH_3$-SCR catalyst. XRD, FTIR, SEM and TEM analyses demonstrated the successful synthesis of a series of "flower-like" LDHs, which are good precursors for the fabrication of highly dispersed $Cu_yMn_zAl_{1-z}O_x$ mixed oxide catalysts. The best catalyst $Cu_2Mn_{0.5}Al_{0.5}O_x$ showed much higher catalytic activity than the control catalyst $Cu_2AlO_x$, Cu-Mn/γ-$Al_2O_3$ and Mn/γ-$Al_2O_3$. The maximum $NO_x$ conversions are 91.2%, 84.2%, 82.6%, and 67.2% for $Cu_2Mn_{0.5}Al_{0.5}O_x$, $Cu_2AlO_x$, Cu-Mn/γ-$Al_2O_3$ and Mn/γ-$Al_2O_3$, respectively. XRD and XPS analyses indicated that the $Cu_2Mn_{0.5}Al_{0.5}O_x$ catalyst mainly contains well dispersed $MnO_2$ and CuO nanoparticles, which are the main active components. In addition, the high concentrations of $Mn^{4+}$ and $Cu^{2+}$ should also be partly responsible for the good performance of $Cu_2Mn_{0.5}Al_{0.5}O_x$ catalyst. $NH_3$-TPD and $H_2$-TPR analyses indicated that $Cu_2Mn_{0.5}Al_{0.5}O_x$ possesses more acid sites and higher reducibility than other catalysts studied in this work. $Cu_2Mn_{0.5}Al_{0.5}O_x$ catalyst was also demonstrated to possess much better $SO_2$ and $H_2O$ resistance than other control catalysts studied in this work. The regeneration studies of deactivated catalysts by thermal treatment at high temperatures indicated that the $NO_x$ conversion of $Cu_2Mn_{0.5}Al_{0.5}O_x$ could be recovered to 84.8%, which is only slightly lower than its initial value (91.2%).

**Acknowledgements**

This work was supported by the Fundamental Research Funds for the Central Universities (2016ZCQ03), the National Natural Science Foundation of China (51622801, 51572029, and 51308045), and the Beijing Excellent Young Scholar (2015000026833ZK11).

**References**


1 W. Tian, H. Yang, X. Fan and X. Zhang, *J. Hazard. Mater.* , 2011, 188, 105-109.
2 S. Zhang, X. Liu, Q. Zhong and Y. Yao, *Catal. Commun.*, 2012, 25, 7-11.
3 G. A. Papapolymerou and L. D. Schmidt, *Langmuir,* 1985, 1, 488-495.
4 M. Kang, E. D. Park, J. M. Kim and J. E. Yie, *Appl. catal. A: general*, 2007, 327, 261-269.
5 J. R. Klovsky, P. B. Koradia and C. T. Lim, *Ind. Eng. Chem. Prod. Res. Dev.*, 1980, 19, 218-225.
6 H. Bosch and F. J. I. G. Janssen, *Catal. Today,* 1988, 2, 369-379.
7 G. Busca, L. Lietti, G. Ramis and F. Berti, *Appl. Catal. B: Environ.,* 1998, 18, 1-36.
8 W. S. Kijlstra, J. C. M. L. Daamen, J. M. van de Graaf, B. van der Linden, E. K. Poels and A. Bliek, *Appl. Catal. B: Environ.,* 1996, 7, 337-357.
9 J. Muniz, G. Marban and A. B. Fuertes, *Appl. Catal. B: Environ.,* 2000, 27, 27-36.
10 L. Singoredjo, R. Korver, F. Kapteijn and J. Moulijn, *Appl. Catal. B: Environ.*, 1992, 1, 297-316.
11 U. Bentrup, A. Brückner, M. Richter and R. Fricke, *Appl. Catal. B: Environ.*, 2001, 32, 229-241.
12 G. Qi, R. T. Yang and R. Chang, *Catal. Lett.*, 2003, 87, 67-71.
13 P. G. Smirniotis, D. A. Peña and B. S. Uphade, *Angew. Chem. Int. Ed.*, 2001, 40, 2479-2482.
14 G. Qi and R. T. Yang, *Appl. Catal. B: Environ.*, 2003, 44, 217-225.
15 M. Wallin, S. Forser, P. Thormählen and M. Skoglundh, *Ind. Eng. Chem. Res.*, 2004, 43, 7723-7731.
16 W. S. Kijlstra, D. S. Brands and E. K. Poels, *J. Catal.*, 1997, 171, 208-218.
17 B. Thirupathi and P. G. Smirniotis, *J. Catal.*, 2012, 288, 74-83.
18 Z. Wu, R. Jin, Y. Liu and H. Wang, *Catal. Commun.*, 2008, 9, 2217-2220.
19 B. Thirupathi and P. G. Smirniotis, *Appl. Catal. B: Environ.*, 2011, 110, 195-206.
20 M. Kang, E. D. Park, J. M. Kim and J. E. Yie, *Catal. Today,* 2006, 111, 236-241.
21 B. Jiang, Z. Li and S. C. Lee, *Chem. Eng. J.*, 2013, 225, 52-58.
22 M. Qiu, S. Zhan, H. Yu, D. Zhu and S. Wang, *Nanoscale*, 2015, 7, 2568-2577.
23 G. Xie, Z. Liu, Z. Zhu, Q. Liu, J. Ge and Z. Huang, *J. Catal.*, 2004, 224, 36-41.
24 G. Xie, Z. Liu, Z. Zhu, Q. Liu, J. Ge and Z. Huang, *J. Catal.*, 2004, 224, 42-49.
25 J. Wang, X. Mei, L. Huang, Q. Zheng, Y. Qiao, K. Zang, S. Mao, R. Yang, Z. Zhang, Y. Gao, Z. Guo, Z. Huang and Q. Wang, *J. Energy. Chem.*, 2015, 24, 127-137.
26 Q. Wang, H. H. Tay, D. J. W. Ng, L. Chen, Y. Liu, J. Chang, Z. Zhong, J. Luo and A. Borgna, *ChemSusChem*, 2010, 3, 965-973.
27 Q. Wang, Y. Gao, J. Luo, Z. Zhong, A. Borgna, Z. Guo and D. O'Hare, *RSC Advances*, 2013, 3, 3414-3420.

28 Q. Wang, H. H. Tay, L. Chen, Y. Liu, J. Chang, Z. Zhong, J. Luo and A. Borgna, *J. Nanoeng. Nanomanuf.*, 2011, 1, 298-303.
29 Y. Gao, Z. Zhang, J. Wu, X. Yi, A. Zheng, A. Umar, D. O'Hare and Q. Wang, *J. Mater. Chem. A*, 2013, 1, 12782-12790.
30 H. Yan, J. Lu, M. Wei, J. Ma, H. Li, J. He, D. G. Evans and X. Duan, *J. Mol. Struc.Theochem*, 2008, 866, 34-45.
31 F. Liu and H. He, *J. Phys. Chem. C*, 2010, 114, 16929-16936.
32 D. Yuan, X. Li, Q. Zhao, J. Zhao, M. Tadé and S. Liu, *J. Catal.*, 2014, 309, 268-279.
33 C. Gennequin, T. Barakat, H. L. Tidahy, R. Cousin, J. F. Lamonier, A. Aboukaïs and S. Siffert, *Catal. Today*, 2010, 157, 191-197.
34 B. Jiang, Y. Liu and Z. Wu, *J. Hazard. Mater.*, 2009, 162, 1249-1254.
35 M. Yu, C. Li, G. Zeng, Y. Zhou and X. Zhang, *Appl. Surf. Sci.*, 2015, 342, 174-182.
36 W. S. Kijlstra, M. Biervliet, E. K. Poels and A. Bliek, *Appl. Catal. B: Environ.*, 1998, 16, 327-337.
37 R. Mrad, R. Cousin, C. Poupin, A. Aboukaïs and S. Siffert, *Catal. Today*, 2015, 257, 98-103.
38 Z. Wu, B. Jiang and Y. Liu, *Appl. Catal. B: Environ.*, 2008, 79, 347-355.
39 K. Yamazaki, T. Suzuki, N. Takahashi, K. Yokota and M. Sugiura, *Appl. Catal. B: Environ.*, 2001, 30, 459-468.
40 A. S. Reddy, C. S. Gopinath and S. Chilukuri, *J. Catal.*, 2006, 243, 278-291.
41 F. Kapteijn, A. D. Vanlangeveld, J. A. Moulijn, A. Andreini, M. A. Vuurman, A. M. Turek, J.-M. Jehng and I. E. Wachs, *J. Catal.*, 1994, 150, 94-104.
42 X. Tang, J. Li, L. Sun and J. Hao, *Appl. Catal. B: Environ.*, 2010, 99, 156-162.
43 Y. Wu, Y. Lu, C. Song, Z. Ma, S. Xing and Y. Gao, *Catal. Today*, 2013, 201, 32-39.
44 C. Fang, D. Zhang, S. Cai, L. Zhang, L. Huang, H. Li, P. Maitarad, L. Shi, R. Gao and J. Zhang, *Nanoscale*, 2013, 5, 9199-9207.
45 L. Chen, J. Li and M. Ge, *Chem. Eng. J.*, 2011, 170, 531-537.
46 Q. Li, H. Yang, F. Qiu and X. Zhang, *J. hazard. mater.*, 2011, 192, 915-921.
47 F. Liu, H. He, C. Zhang, Z. Feng, L. Zheng, Y. Xie and T. Hu, *Appl. Catal. B: Environ.*, 2010, 96, 408-420.
48 J. Zhu, F. Gao, L. Dong, W. Yu, L. Qi, Z. Wang, L. Dong and Y. Chen, *Appl. Catal. B: Environ.*, 2010, 95, 144-152.
49 B. Liu, Y. Liu, C. Li, W. Hu, P. Jing, Q. Wang and J. Zhang, *Appl. Catal. B: Environ.*, 2012, 127, 47-58.
50 Y. Xiong, C. Tang, X. Yao, L. Zhang, L. Li, X. Wang, Y. Deng, F. Gao and L. Dong, *Appl. Catal. A: general*, 2015, 495, 206-216.
51 Q. Yan, Y. Nie, R. Yang, Y. Cui, H. O, D. and Q. Wang, *Appl. catal. A: general*, 2017, 538, 37-50.
52 Z. Sheng, Y. Hu, J. Xue, X. Wang and W. Liao, *J. Rare Earths*, 2012, 30, 676-682.